PROGRESS REPORT

PRECIPITATION IN RAPIDLY SOLIDIFIED Aℓ-Mn ALLOYS

D. SHECHTMAN AND E. HOROWITZ

THE JOHNS HOPKINS UNIVERSITY
CENTER FOR MATERIALS RESEARCH
BALTIMORE, MARYLAND 21218
(301) 338-7916

DARPA ORDER NO.: MDA 903-81-C-0555 AO 4344
EFFECTIVE DATE: 08-01-81
EXPIRATION DATE: 01-31-84
SPONSORED BY: DEFENSE ADVANCED RESEARCH PROJECTS AGENCY (DARPA)

AUGUST 19

TABLE OF CONTENTS

LIST OF FIGURES

LIST OF FIGURES

EXECUTIVE SUMMARY

This study was performed in collaboration with R. J. Schaefer and F. S. Biancaniello of the Metallurgy Division, National Bureau of Standards. The results summarized here conclude the study of alloy compositions containing 15 wt.% Mn or less. Another study of the same alloy system on alloys of higher manganese concentrations is now in progress and will be reported in the future.

Precipitation at 450°C was studied in melt-spun ribbons containing up to 15 wt.% Mn in solid solution in Aℓ. The as-spun ribbons were microsegregation-free at compositions up to 5 wt.% Mn, but in more concentrated alloys a cellular microstructure was present. Upon annealing, four precipitate phases are observed, some of them being found preferentially on cell boundaries and others within the cells. $Aℓ_6Mn$, G and the G" phase can coexist for long times at 450°C, but the G phase appears to be slightly more stable. A less stable T phase was detected in Aℓ-5 wt.% Mn foils following short annealing periods. The supersaturation of the Aℓ matrix can persist for many hours in alloys containing up to 3 wt.% Mn, but is essentially gone after 1 hour in alloys with 5 wt.% Mn or more.

I. INTRODUCTION

It has been known for many years that solid solutions containing far more than the equilibrium limit of manganese in aluminum can be obtained by rapid solidification [1]. A phase designated G, usually considered to be metastable and with composition corresponding to $Al_{12}Mn$, appears during the annealing of these supersaturated solutions, and at temperatures below about 500°C the G phase can persist for long times in samples which also contain the Al_6Mn phase [2]. Nes, et al., [3] have found two other metastable phases in Al-1.8 wt.% Mn annealed at 460°C. One phase was designated G" and it has an hexagonal lattice with c/a = 1.04, and the other phase G' has a simple cubic structure. The Al-Mn system is of special interest because of the possibility that even concentrated alloys can freeze with microsegregation, as predicted by the theory of morphological stability [4], and because of the very slow rate at which phase equilibrium is established. Unfortunately, none of the previous studies of precipitation in this system has covered the wide range of solid solution compositions which is attainable by rapid solidification.

Extensive reviews [5,6,7] covering many aspects of the study of rapidly solidified aluminum alloys point out that a solid solubility extension has been observed in almost every system which has been investigated. For alloying elements such as Fe or Ni, which have extremely low maximum

equilibrium solid solubilities, the observed solubilities in rapidly solidified aluminum lie far beyond any reasonable metastable extension of the solidus and thus indicate a non-equilibrium reaction at the solid-liquid interface. In contrast, manganese has a high solubility in aluminum and if the formation of competing phases can be avoided, large extensions of the solubility limit would be expected even without any departure from equilibrium at the solid-liquid interface.

On the basis of interface equilibrium, the theory of morphological stability predicts an absolute stability regime in which plane-front microsegregation-free solidification of an alloy is stabilized by surface energy effects at sufficiently high solidification velocities. In the aluminum-manganese system the velocity required to produce this effect is predicted to be relatively low because of the high value of the solute partition coefficient [8]. By this mechanism, rapid solidification processing could produce rather concentrated Aℓ-Mn alloys without microsegregation. For example, a planar solid/liquid interface is predicted to be stable in an alloy containing 10 wt.% Mn when the solidification velocity is 6×10^{-2} m/s or greater, provided that at least a moderate positive temperature gradient is present in the liquid. At comparable solidification velocities, elements having low distribution coefficients (such as Fe) are predicted to be destabilizing even at concentrations $<<1$ wt.%.

At higher solidification velocities, it is expected that the interface equilibrium is no longer maintained, and micro-segregation-free solidification can be obtained even in systems having very low equilibrium partition coefficients [9].

The solidification microstructure plays an important role in the precipitation process in Aℓ-Mn alloys because it influences the distribution of the various precipitating phases. Because of the slow rate at which these phases displace one another, the solidification microstructure thus determines which of these phases dominates at various stages of annealing. We report here a study of the relationships between the microstructures formed in rapidly solidified Aℓ-Mn alloys and the precipitation processes in these alloys.

II. EXPERIMENTAL

A. Sample Preparation

Alloy buttons with Mn concentrations of 0.1, 1, 2, 3, 5, 9, 12, and 15 wt.% Mn were prepared by arc melting, using 99.999% Aℓ and 99.95% Mn. For melt spinning, small pieces cut from these buttons were induction heated in zirconia-coated quartz tubes. Immediately upon melting, the metal was squirted onto a copper melt-spinning wheel, 10 cm in diameter, which rotated at 7000 rpm. The process was carried out under helium at atmospheric pressure. The ribbons were typically 2 mm wide and 40-50 μm thick. For annealing, the ribbons were sealed in borosilicate glass ampoules with 1/2 atmosphere of helium.

B. X-ray Studies

Lattice parameters were determined by measurements on an x-ray diffractometer, using filtered CuKα radiation. A Nelson-Reiley procedure was used to obtain the lattice parameter from the measurements of the diffraction peaks. Simultaneous measurement of diffraction peaks from powdered high purity silicon were used as a normalization standard. The relative abundance of precipitate phases was evaluated by measuring the amplitude of the strongest peaks.

C. Electron Microscopy

Microstructural studies were performed in a 120 kv scanning transmission electron microscope. The ribbons were thinned by jet electropolishing in a standard solution of 1.5% HNO_3 and 5% $HC1O_4$ in methanol at -30°C.

III. RESULTS

A. Phase Identification

Four phases have been identified by TEM in the as-spun and in the heat treated ribbons, in addition to the aluminum matrix. The crystallography of these phases will be shown now while their morphology and occurrence will be discussed later in this paper.

Al_6Mn - This phase is shown in Fig. 1. The particles are generally globular, do not show any preference in growth direction within the aluminum matrix and can be found either on subgrain boundaries or within the subgrains depending upon composition and heat treatment. The electron diffraction patterns obtained from this phase agree with its established crystallography [10] except for the (001) reflection which is forbidden by the symmetry of the crystal but clearly observed on the diffraction patterns. This may indicate a metastable structure of this equilibrium phase.

G Phase - This phase is semicoherent with the aluminum matrix and, therefore, surrounded by misfit dislocations as can be seen in Fig. 2. The orientation relationship between the G phase and the aluminum matrix was reported before [3] as $(310)_G \,||\, (111)_{Al}$ and $(111)_G \,||\, (310)_{Al}$ and our findings support it.

G" Phase - This phase was analyzed [3] as hexagonal with lattice parameter a = 0.754 nm, and c/a = 1.04. It is faulted parallel to the basal plane and thus its diffraction

pattern contains streaks in the c direction. The plate normal of these particles is parallel to the c direction (Fig. 3). We have determined the orientation relationship between the G" phase and the aluminum matrix (Fig. 3) to be $(0113)_{G"}||(111)_{Al}$ $[2110]_{G"}||[110]_{Al}$.

T Phase - This phase has the shape of an elongated plate, and was not completely characterized. It has a complex faulted structure (Fig. 4) with the faults forming on planes perpen ·u- lar to its length, and it does not correspond to any previc v reported phase. The crystallography of this phase and its orientation relationship with the matrix will be studied in the future.

The G' phase of Nes, et al. [3], which was believed to be associated with impurities, was not detected in our samples.

On the x-ray diffraction charts, peaks are seen corresponding to the Al_6Mn phase [10] and the G phase [2, 11, 12, 13, 14]: no peaks are seen which do not correspond to reflections reported in the literature for these phases. Table I presents a listing of the x-ray lattice parameter and precipitate phase results.

B. As-Spun Ribbons

The 3 wt.% Mn alloy is a supersaturated solid solution formed without microsegregation. Its microstructure consists of cell-free grains containing a high dislocation density (Fig. 5). At 5 wt.% Mn, two different runs on the melt spinner

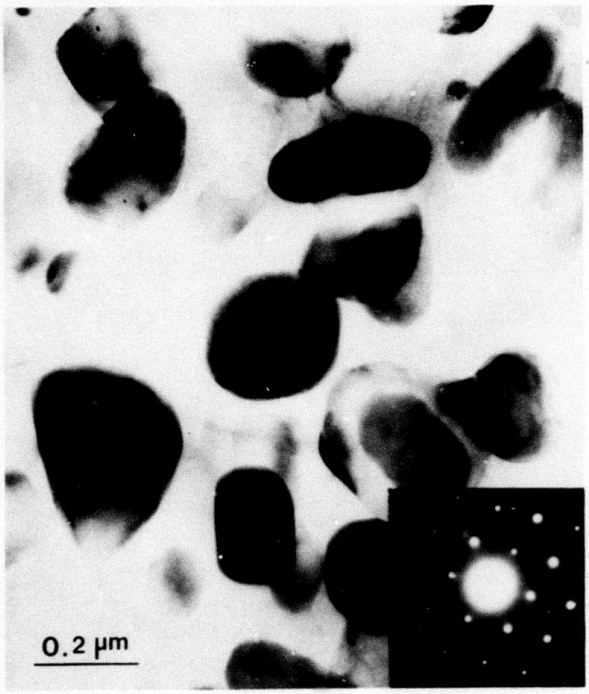

FIGURE 1.
$A\ell_6Mn$ particles. The diffraction pattern represents a [101] zone axis.

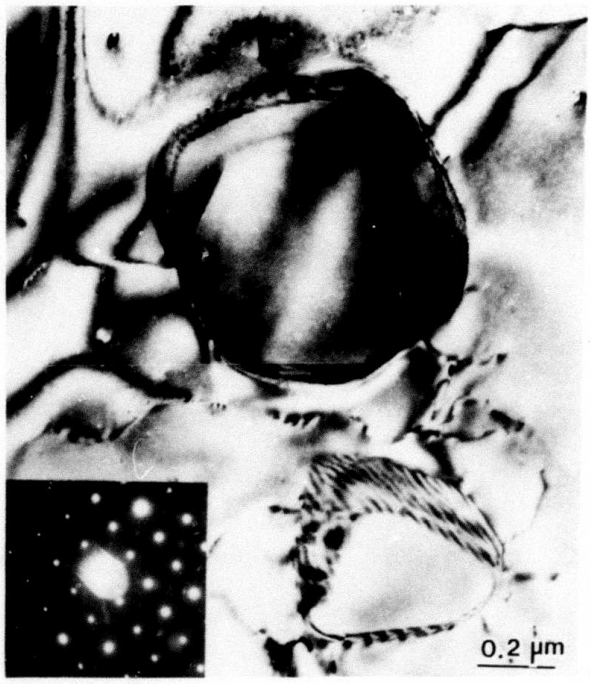

FIGURE 2.
G phase particles. The diffraction pattern represents a [001] zone axis.

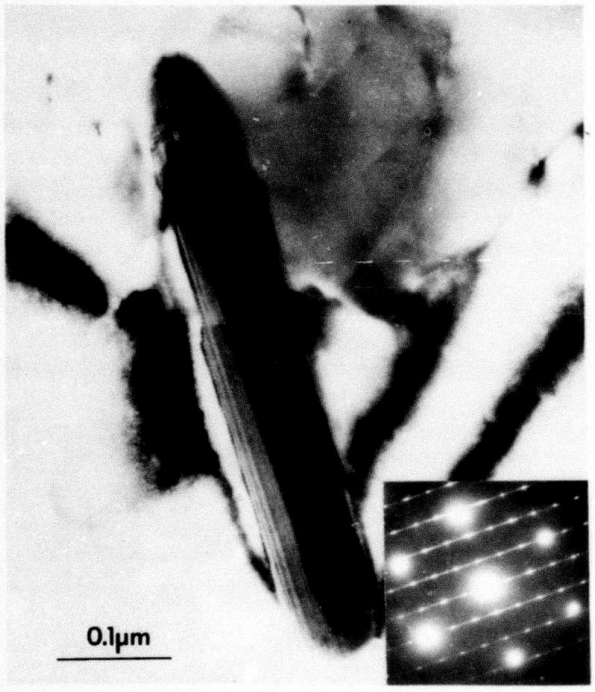

FIGURE 3.
G" phase particle. The diffraction pattern represents a [110] Aluminum zone axis and (2110) G" zone axis.

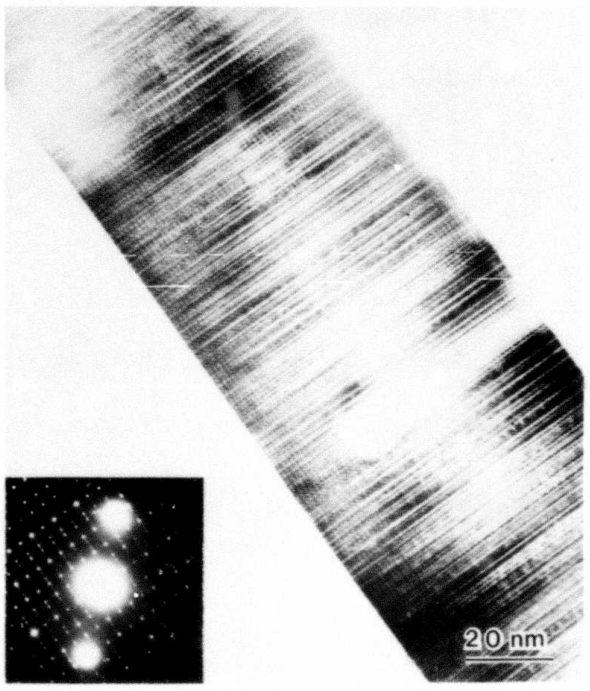

FIGURE 4.
T phase particles. Note faults perpendicular to its length and the resulting complex diffraction pattern.

TABLE I. SUMMARY OF X-RAY DIFFRACTION RESULTS

Wt.% Mn	Time at 450°C (hrs.)	Lattice Parameter a(nm)	Al_6Mn Intensity*	G Intensity*
0.1	0	0.40492	0	0
	3	0.40495	0	0
1.0	0	0.40460	0	0
	1	0.40475	0	0
	16	0.40475	0	T
2.0	0	0.40424	0	0
	1	0.40440	VW	0
	3	0.40452	0	0
	16	0.40467	VW	0
	48	0.40487	VW	VW
3.0	0	0.40392	0	0
	1	0.40392	VW	0
	1	0.40409	W	0
	3	0.40423	T	0
	3	0.40406	VW	0
	16	0.40485	VW	W
	48		VW	S
	92	0.40488	VW	S
5.0 (thin)	0	0.40301	0	0
	1	0.40496	VW	0
	3	0.40502	W	0
	16	0.40493	M	0
	48		M	0
	65		M	0
	87		W	0
5.0 (thick)	0	0.40352		
	1	0.40494	M	0
	3	0.40499	W	M
	16	0.40504	M	S
	48		VW	VS
9.0	0	0.40238	0	0
	0.08	0.40311	VW	0
	0.17	0.40459	M	0
	0.33	0.40477	M	0
	1	0.40500	M	0
	3	0.40501	S	0
	16	0.40511	M	W

Table I (cont.)

Wt.% Mn	Time at 450°C (hrs.)	Lattice Parameter a(nm)	Al_6Mn Intensity*	G Intensity*
12.0	0	0.40157	0	0
	0	0.40157	0	0
	0	0.40157	0	0
	0	0.40174	0	0
	1	0.40512	S	0
	3	0.40523	S	T
	16	0.40537	S	S
	22		M	VS
	48		M	VS
15.0	0	3.9994 4.0371		
	1		W	S
	6		W	VS

*Intensities: 0 = not detected, T = trace, VW = very weak, w = weak, m = medium, s = strong, vs = very strong.

produced distinctly different ribbons; a thin, narrow ribbon and a thicker, wider ribbon which was produced when the nozzle of the melt spinner was moved closer to the wheel. Most of the ribbons at the other concentrations were intermediate in thickness between the two sets produced at 5 wt.% Mn. The thin (35 μm maximum thickness) and the thick (55 μm) ribbon of the 5 wt.% Mn alloy are distinctively different from one another. The microstructure of the thin ribbon is cell-free and resembles that of the Aℓ-3 wt.% Mn alloy. The thick ribbon is cellular, with cell size about 2 μm, and contains unidentified precipitates at the cell boundaries (Fig. 6). These two types of microstructure are probably related to differences in the solidification velocities of the ribbons.

The 9 wt.% Mn alloy has a cellular microstructure (Fig. 7) with average cell size of 1 μm, and it contains fine precipitates at the cell boundaries. The alloys containing 12 and 15 wt.% Mn are both cellular in their as-spun condition. The cell boundaries contain fine precipitates but the cell interiors are mostly free from any precipitation (Figs. 8 and 9). The contrast difference in the cells indicates that the cell boundary is also a subgrain boundary, which probably stems from the strain generated by the fine precipitation at the cell boundary. This also supports the conclusion that the particles at the cell boundary result from a solid state decomposition of the highly supersaturated cell boundary. In addition, the 15 wt.% Mn

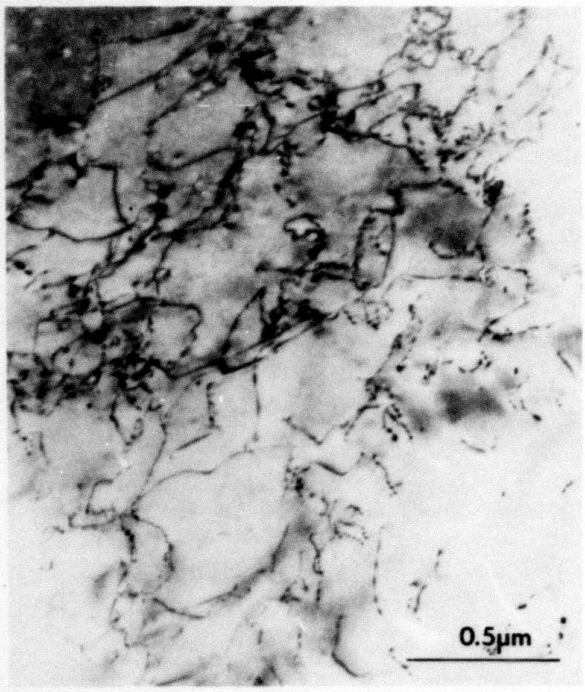

FIGURE 5.
As spun ribbon of Aℓ-3 wt.% Mn alloy. The microstructure shows complete solubility of the manganese.

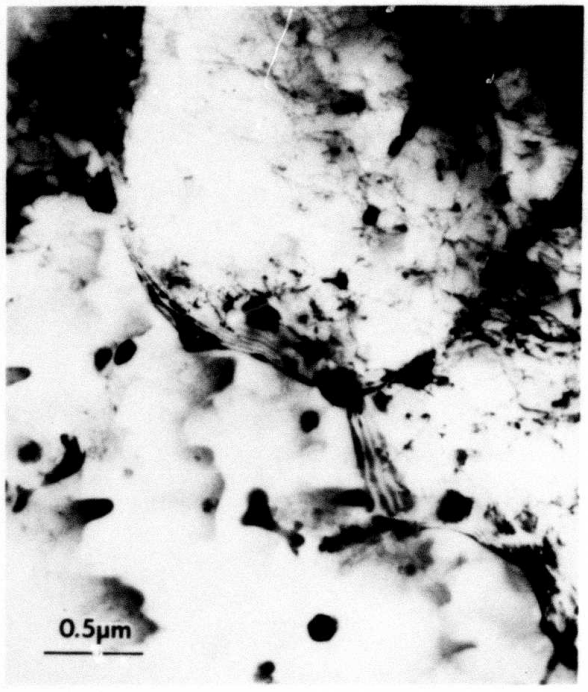

FIGURE 6.
As spun thick ribbon of Aℓ-5 wt.% alloy. Particles are seen at cell boundaries.

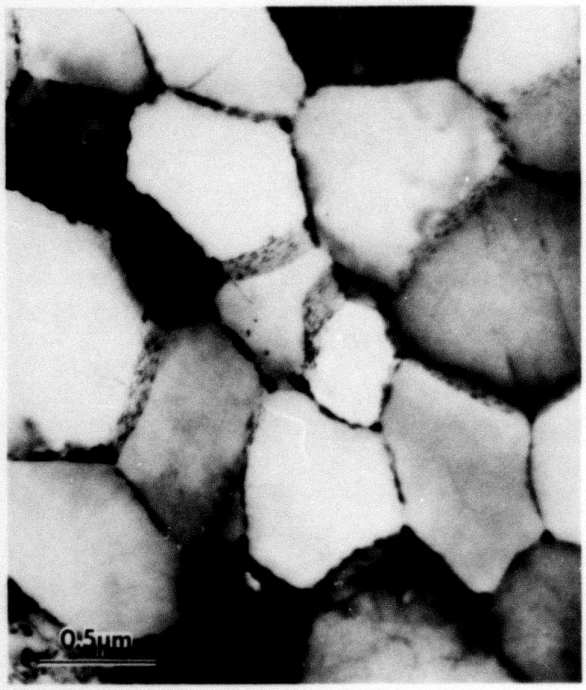

FIGURE 7.
As spun ribbon of Aℓ-9 wt.% Mn alloy. A cellular microstructure with particles at the cell boundary is observed.

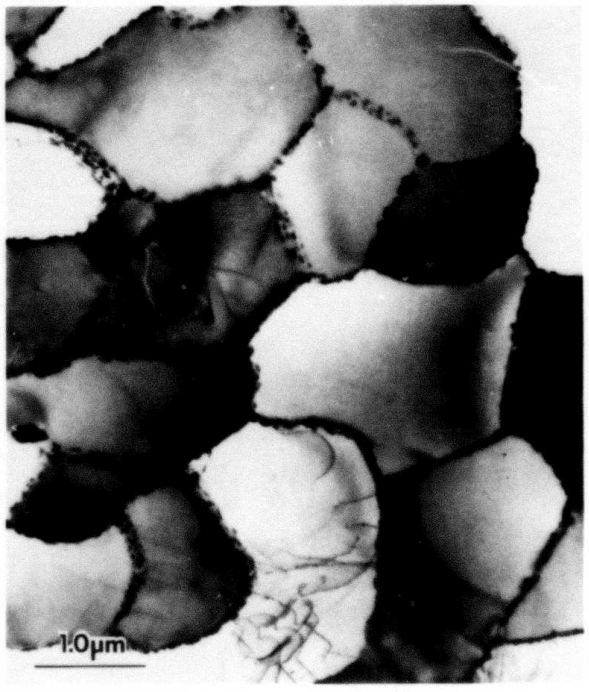

FIGURE 8.
As spun ribbon of Aℓ-12 wt.% Mn alloy. A cellular microstructure with particles at the cell boundaries is observed.

alloy contains regions with a much finer cell spacing and higher density of precipitates, which could indicate a two-phase solidification process.

In the as-spun ribbons, only the aluminum phase is seen on the x-ray diffraction charts at compositions up to 12 wt.% Mn. Any other phases present are too small in volume to be detected. The lattice parameter (Fig. 10) decreases steadily with increasing Mn content. At 12 wt.% Mn the diffraction peaks of the as-spun ribbons are sharp but have a distinct tail on the low-angle side, indicative of a composition which is mostly uniform but contains local regions with a range of lower compositions. At 15 wt.% Mn, however, the as-spun ribbon shows two separate sets of Aℓ peaks which correspond to material containing two different concentrations of Mn in solid solution. The peaks from the material containing the higher concentration of Mn are stronger relative to those from the less concentrated material on the side of the ribbon which was adjacent to the melt spinner wheel. In addition, the (111) and (222) reflections from the more concentrated material were especially intense, indicating a preferred orientation. Two weak peaks, attributed to precipitates, were also present but the phase could not be identified. Figure 10 shows lines representing previously reported results [1,15,16,17] for lattice parameters in rapidly quenched Aℓ-Mn. Our own results are shown as solid points for samples in which no cellular structure was observed by electron microscopy and as open circles for samples with

cellular microstructures. The former group of points may be taken to represent the true concentration dependence of the lattice parameter, while the data from cellular samples are derived from lattices containing somewhat less than the normal concentration of Mn in solid solution, with the remainder of the Mn being incorporated into micro-precipitates at the cell or grain boundaries. Note that the cell-free thin 5% Mn ribbon has a lattice parameter distinctly smaller than that of the thicker ribbon. This is consistent with the supposition that in the thicker ribbon the solidification rate was not great enough to incorporate all of the manganese into the supersaturated solid solution. Note also that the two lattice parameters observed in the 15 wt.% Mn sample indicate solid solution compositions of approximately 14 wt.% Mn and 3 wt.% Mn.

C. Heat Treated Ribbons

Up to 3 wt.% Mn

Following 1 hour at 450°C, TEM reveals that elongated Al_6Mn particles precipitate along subgrain boundaries of the Al-3 wt.% Mn. The subgrains contain a high density of dislocations (Fig. 11) and scattered events of precipitation can be observed in some of them.

A prolonged exposure of the 3 wt.% Mn alloy of 92 hours at 450°C results in three well defined types of precipitates. The first, globular in shape and up to 1 μm in diameter, was identified as G phase. The G phase particles have a high degree of coherence with the aluminum matrix as can be seen

both in the diffraction pattern and the presence of misfit dislocations at the semi-coherent boundary (Fig. 12). The second phase, consisting of elongated particles up to 2 μm in length, was identified as G" phase. The G" phase is faulted and the planar faults are perpendicular to the axis of its hexagonal structure, as indicated before [3]. The third phase was identified as Al_6Mn. The Al_6Mn particles are not found on subgrain boundaries, probably due to grain boundary mobility in the annealing process.

X-ray measurements of the lattice parameter of the Al phase showed that in the ribbons containing 3 wt.% Mn or less, the supersaturation disappeared very slowly (Fig. 13). In the 2 and 3 wt.%Mn alloys, Al_6Mn could be detected in the x-ray diffraction charts after 1 hour at 450°C, but the peaks from this phase were very weak and remained so after much longer anneals. Very weak G peaks first appeared after 48 hours in the 2 wt.% Mn alloy, whereas in the 3 wt.% Mn alloy, weak G phase peaks first appeared at 16 hours and became strong at 48 hours.

5 wt.% Mn

The thick and thin ribbons of the Al-5 wt.% Mn alloy were heat treated for periods of 1 to 87 hours at 450°C. The microstructure of the ribbons following 1 hour at this temperature is shown by TEM to contain Al_6Mn particles along subgrain boundaries and a diffused population of fine T type platelets

within the grains (Fig. 14) except in a depleted zone adjacent to the subgrain boundaries. The T platelets are typically 100 to 300 nm long and 10 to 20 nm thick. The microstructure of the thick ribbon is different from the thin one in two ways. The Al_6Mn particles at its subgrain boundaries are more globular and the depleted zone is typically 0.3 to 1 μm thick compared to 0.1 to 0.3 μm in the thin ribbons. These differences diminish at longer exposure times.

Specimens of both the thick and the thin ribbons that were heat treated for 3 hours at 450°C show some precipitate coarsening but are qualitatively identical to the ones heat treated for one hour. Following exposure of 16 hours more coarsening is observed (Fig. 15) and after 48 hours or 65 hours the depleted zone comprises about 50% of the volume of the ribbon (Fig. 16). A comparison between the microstructures developed after 1 hour and 48 hours at 450 (Figs. 14 and 16) reveals the following: The T phase particles are metastable at this temperature, but they do not seem to be a precursor to the Al_6Mn. The Al_6Mn particles grow and become globular in time, and most of them are found on subgrain boundaries, with only a small proportion found within the grains. We tend to attribute the latter to subgrain migration rather than to a possible phase transformation between the T phase and the Al_6Mn.

X-ray diffraction reveals that the supersaturation was essentially gone after 1 hour (Fig. 13) for both the thin and thick ribbons. The long-time development of the dif-

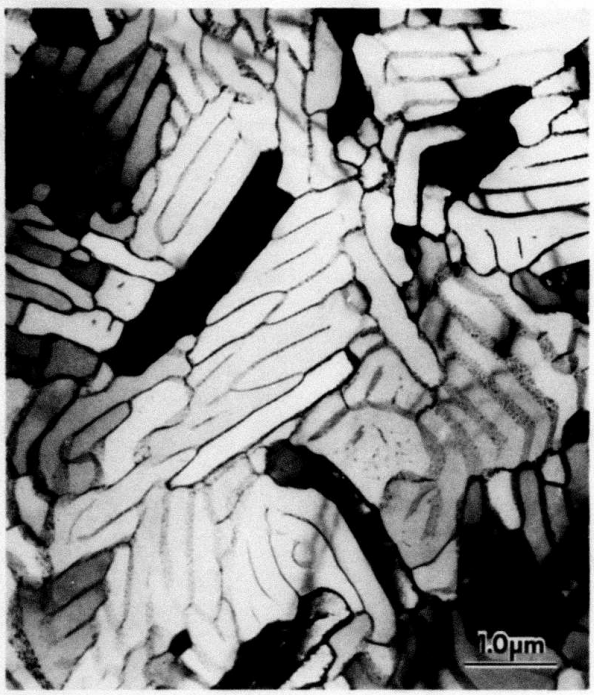

FIGURE 9.
As spun ribbon of Aℓ-15 wt.% Mn alloy. Note the contrast difference between cells indicating that the cells are also subgrains.

FIGURE 11.
$Aℓ_6Mn$ particles at cell boundary of Aℓ-3 wt.% Mn alloy annealed 1 hour at 450°C.

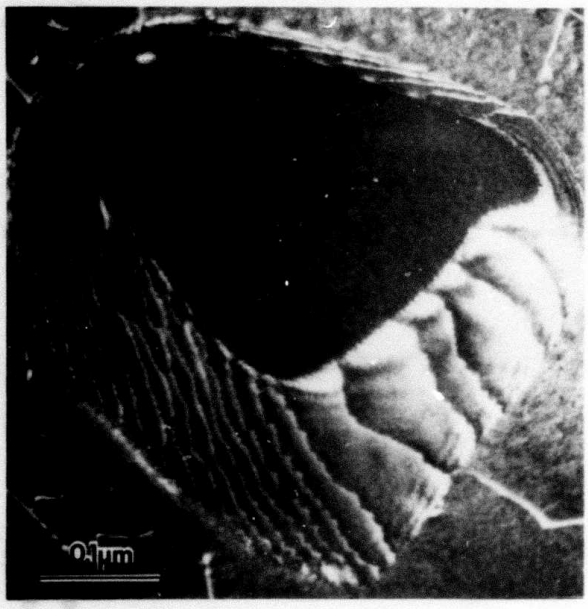

FIGURE 12.
Misfit dislocations at the G phase-aluminum phase boundary (dark field, weak beam).

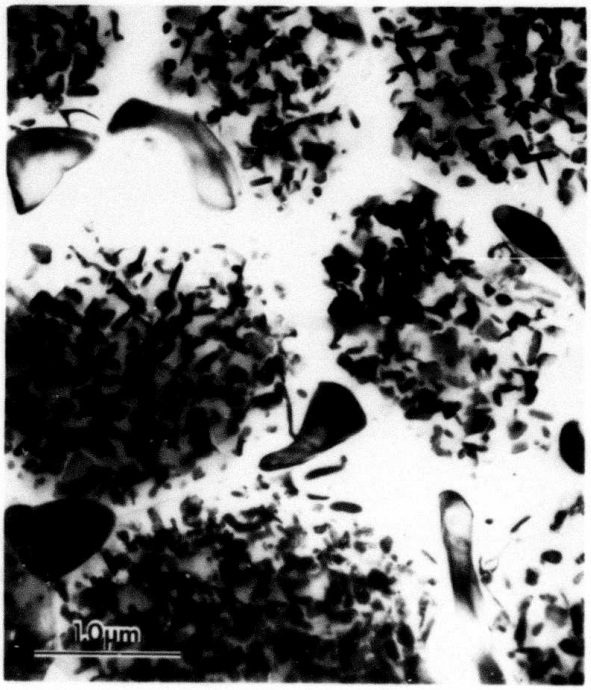

FIGURE 14.
The Aℓ-5 wt.% Mn alloy following 1 hour at 450°C containing $Aℓ_6Mn$ particles along subgrain boundaries and T phase platelets within the grains.

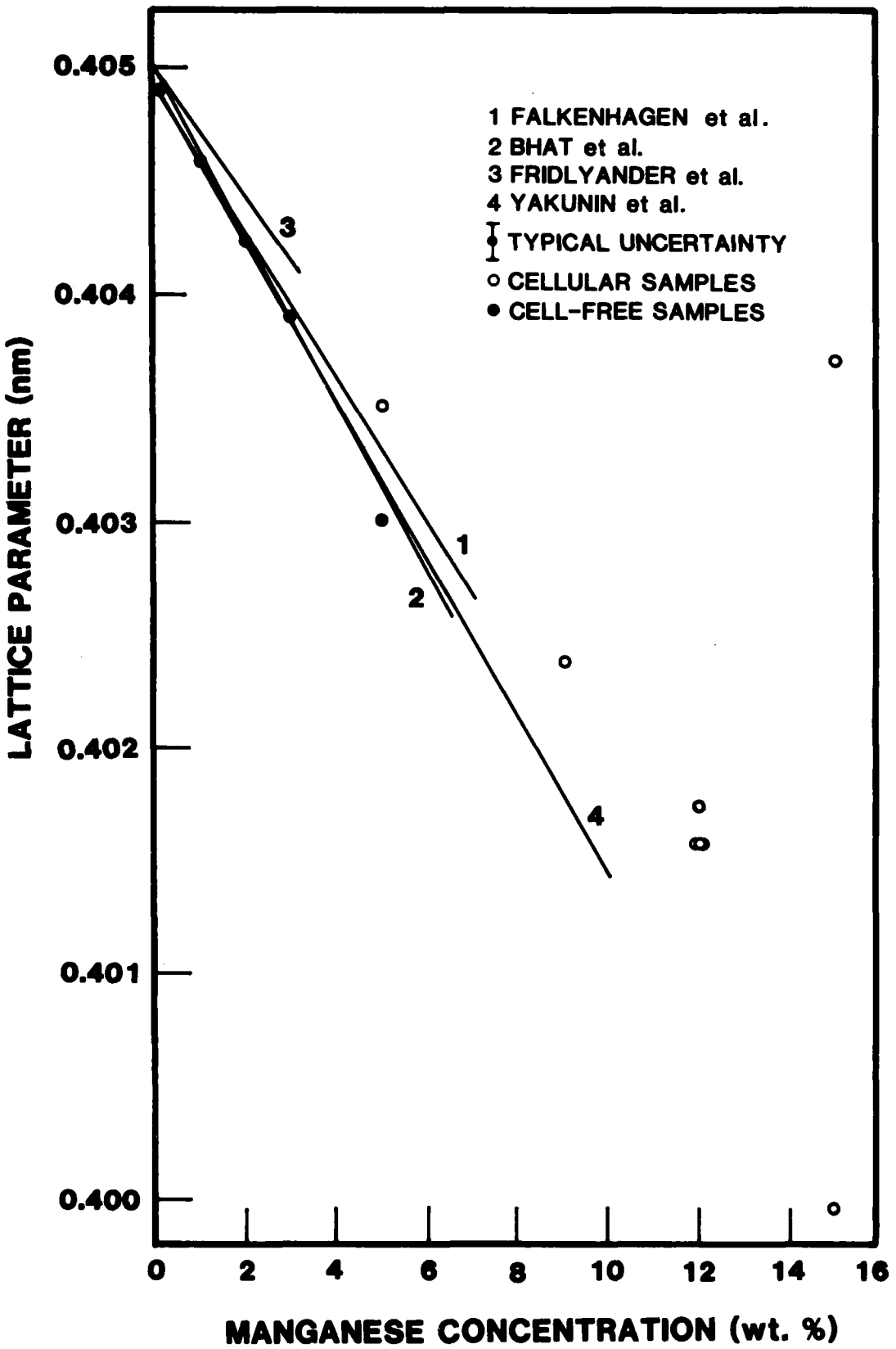

FIGURE 10.
X-ray lattice parameter of as spun Aℓ-Mn ribbons compared to results of Falkenbagen et al. [1], Bhát et al. [17], Fridylander et al. [15] and Yakunin et al. [16].

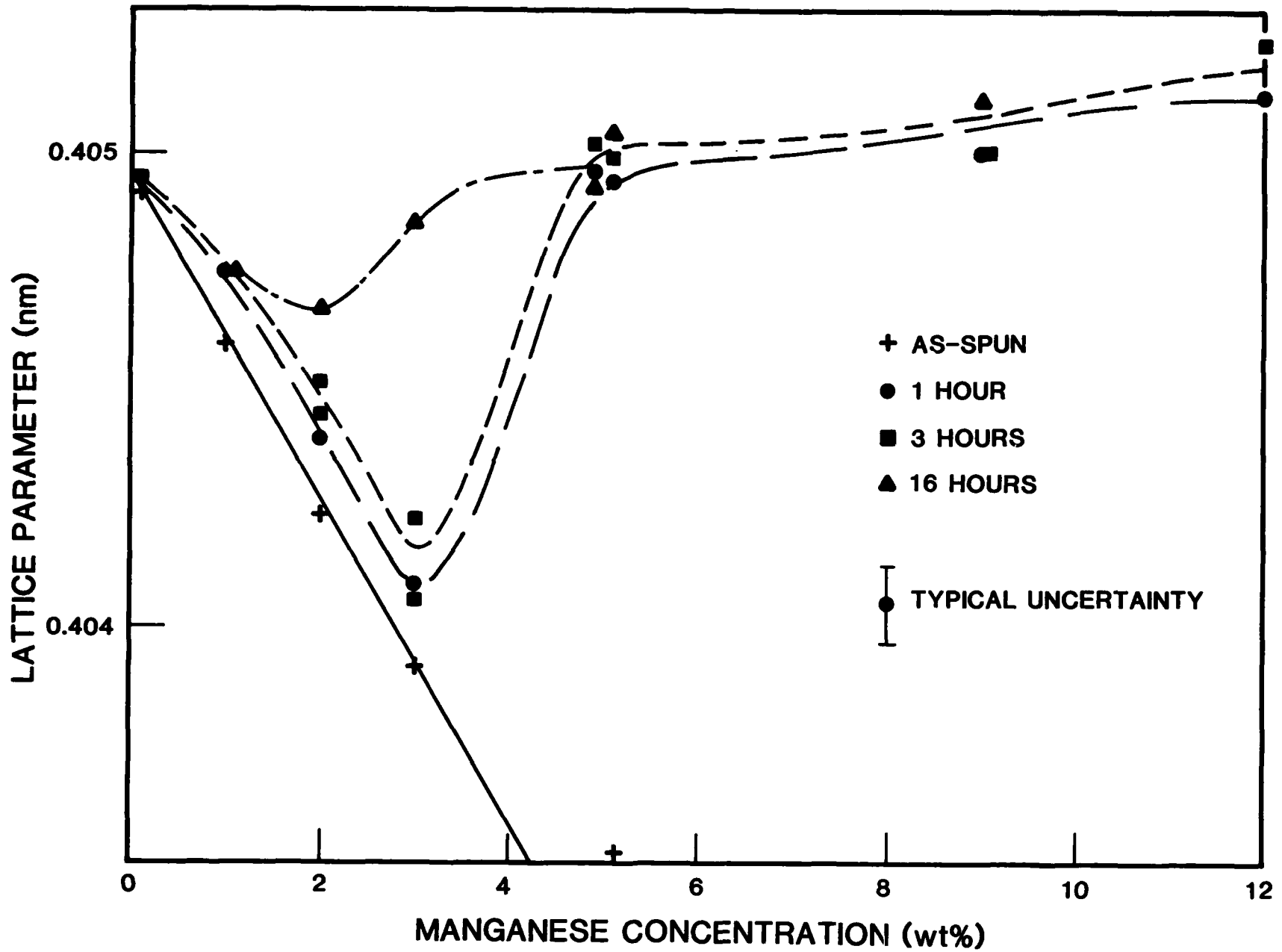

FIGURE 13.
Lattice parameter of Al-Mn ribbons at different annealing times (x-ray diffraction measurements).

fraction peaks from the precipitate phases was dramatically different in the two cases. After one hour, both ribbons showed only Al_6Mn, and in the thin ribbon only this precipitate is seen even after the longest anneals (87 hours). In the thick ribbon, contrastingly, the G phase appears after 3 hours and steadily gains in strength until at 48 hours it is very strong and the Al_6Mn has decreased to a very weak level.

It is apparent from the results that the T phase precipitates either yield an x-ray diffraction pattern not clearly distinguishable from that of the G phase, or that they are too small to be detected by x-ray diffraction while the G phase particles are confined to parts of the ribbon not observed by TEM. Possible reasons that the two methods of analysis yield different readings of the relative abundance of the phases present will be considered in the discussion section.

9 wt.% Mn

Several heat treated ribbons of the 9 wt.% Mn alloy were studied by TEM. After 5 minutes at 450°C two phases are observed in the aluminum matrix (Fig. 17). One phase forms on subgrain boundaries, and is surrounded by a depleted zone. It is globular in shape with size averaging 0.5 μm in diameter. The second phase forms within the grain. These particles are needle-like in shape and measure up to 0.5 μm in length and 10 nm in thickness. Neither phase could be identified.

Following a heat treatment of 1 hour, Al_6Mn particles are seen within the grains (Fig. 18) while most of the needle like phase disappears. After 16 hours at 450°C the Al_6Mn particles within the grains are about 0.5 μm long and large particles of G phase outline the subgrain boundaries (Fig. 19). The x-ray diffraction patterns showed Al_6Mn after only 5 minutes, but the G phase was first seen after a 16 hour heat treatment. The lattice parameter measurement reveals the rapid disappearance of the supersaturation during annealing of the 9 wt.% Mn alloy at 450°C, as shown in Fig. 20.

12 wt.% Mn

Following 1 hour at 450°C, Al_6Mn particles averaging 0.25 μm in length are formed in the aluminum matrix (Fig. 21). These particles coarsen to about 0.5 μm following 3 hours at this temperature. A longer exposure of 22 hours results in the microstructure shown in Fig. 22. The phases were identified as follows: an aluminum phase containing Al_6Mn particles and a G phase which contains a low density of aluminum particles.

The Al_6Mn x-ray diffraction peaks are strong after a 1 hour heat treatment, and a trace of the G phase is first seen at 3 hours. After 48 hours, the G phase peaks are very strong and the Al_6Mn peaks have diminished slightly.

15 wt.% Mn

Following 6 hours at 450°C the microstructure of the ribbon consists of three phases. Aluminum grains which contain

Al_6Mn particles are shown in Fig. 23a. These particles are about 1 μm in size and their volume fraction is about 50%. Other grains are G phase and they contain Al_6Mn and aluminum particles, the size of which is about 300nm (Fig. 23b). The volume fraction of the particles is smaller in the G grains than in the aluminum grains. The x-ray diffraction pattern also shows Al, G, and Al_6Mn.

FIGURE 15.
Coarsening of the T phase in Aℓ-5 wt.% Mn annealed for 16 hours at 450° C.

FIGURE 16.
Aℓ-5 wt.% Mn alloy following annealing for 65 hours at 450° C. T phase particles are found only in the center of the subgrains, and the depleted zone has grown.

FIGURE 17.
The microstructure of the Aℓ-9 wt.% Mn alloy following 5 min. at 450° C.

FIGURE 18.
$Aℓ_6Mn$ particles in the Aℓ-9 wt.% Mn following 1 hour at 450° C.

FIGURE 19.
The Aℓ-9 wt.% Mn alloy following 16 hours at 450° C containing $Aℓ_6Mn$ particles within the grains and almost continuous G phase at subgrain boundaries.

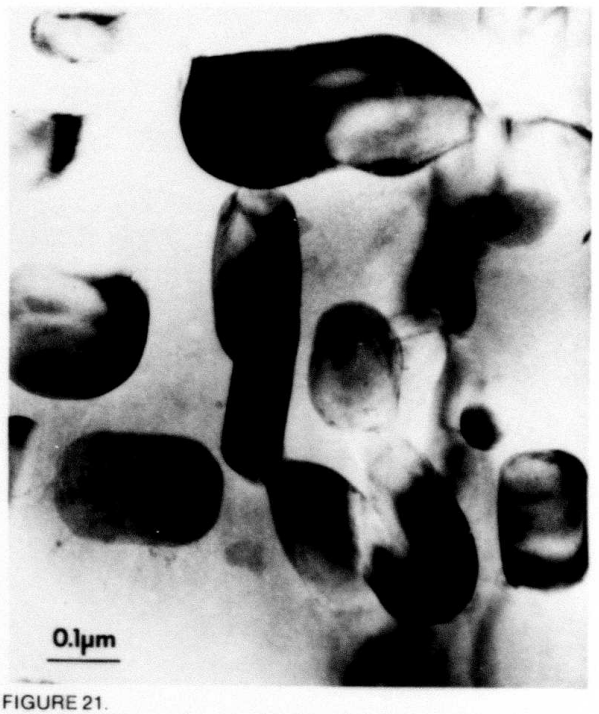

FIGURE 21.
Coarse $Aℓ_6Mn$ particles in Aℓ-12 wt.% Mn following 1 hour at 450° C.

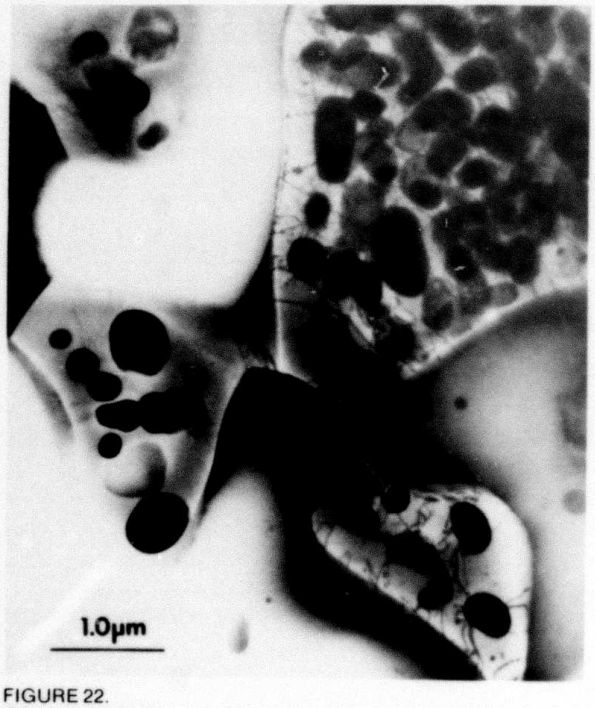

FIGURE 22.
The microstructure of Aℓ-12 wt.% Mn following 22 hours at 450° C containing three phases: $Aℓ_6Mn$ particles in aluminum grains and aluminum particles in the G grains.

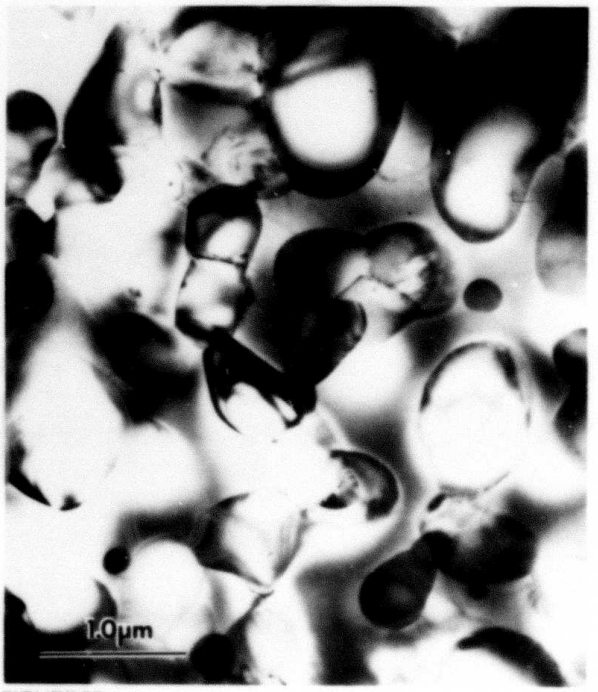

FIGURE 23a.
$Aℓ_6Mn$ particles in aluminum matrix. The microstructure of Aℓ-15 wt.% Mn following 6 hours at 450° C.

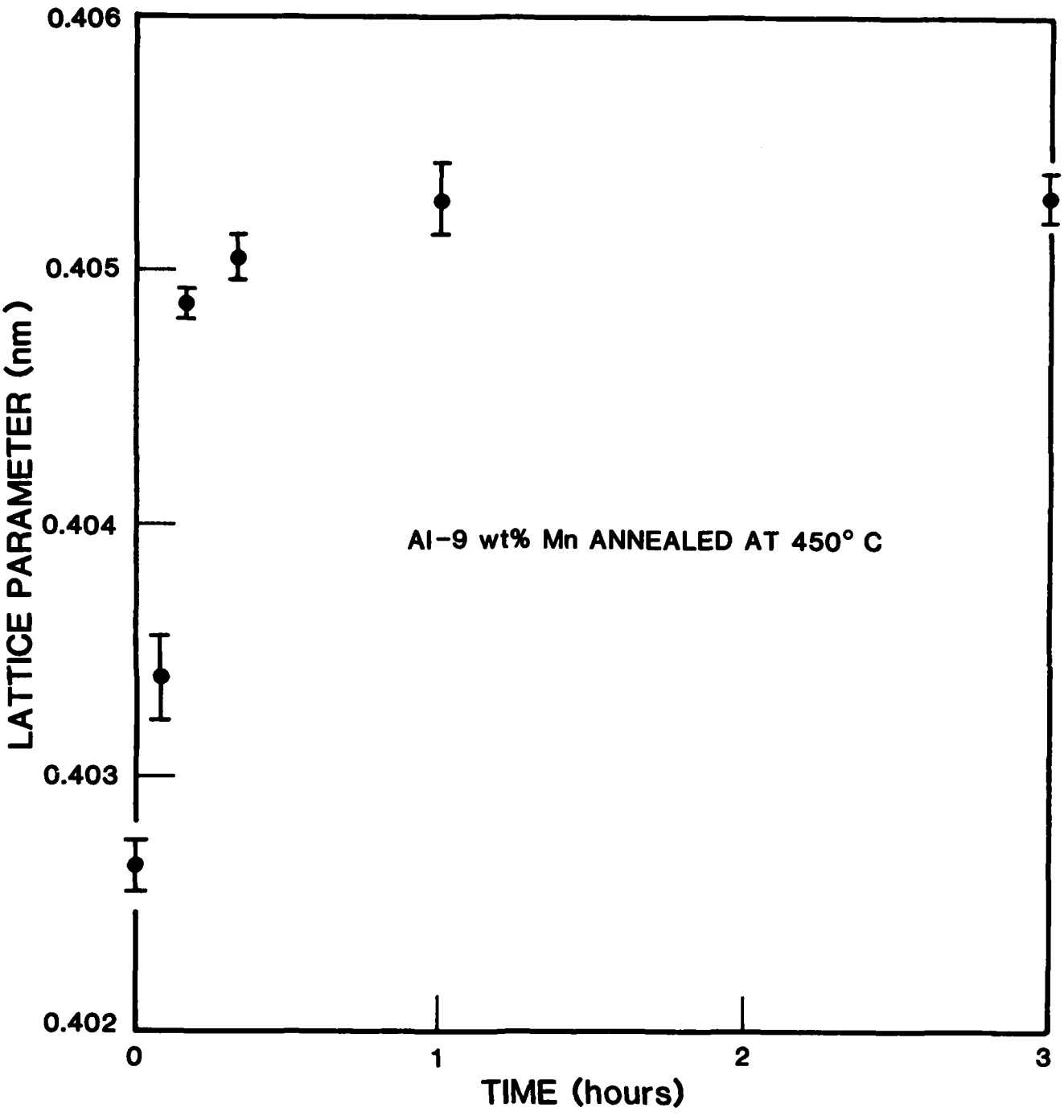

FIGURE 20.
X-ray lattice parameter measurements of Aℓ-9 wt.% Mn as a function of annealing time.

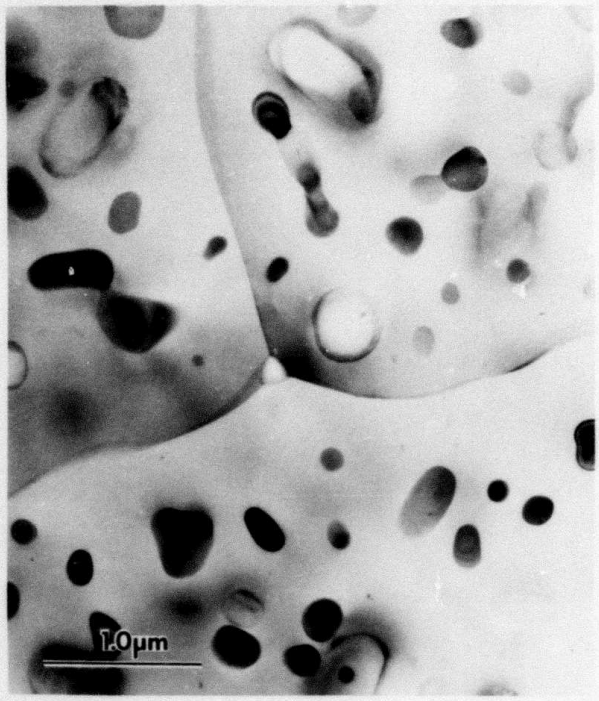

FIGURE 23b.
Al_6Mn and aluminum particles are found in G grains.

IV. DISCUSSION

Melt-spun ribbons are a convenient form of rapidly solidified material for transmission electron microscopy, because they can be thinned for examination without any previous cutting or sectioning operations. They are also convenient for x-ray diffraction in that they can be simply attached to a glass microscope slide with double-stick tape for mounting in a diffractometer. The TEM reveals the microstructural features including the identity of the phases and their distribution, while the x-ray diffraction reveals the lattice parameters and the relative overall abundance of the phases.

In some cases the two methods gave different indications of the occurrence and abundance of the phases, and several factors could explain this apparent discrepancy. Precipitate phases will yield measurable x-ray diffraction peaks only if they constitute at least a few percent of the sample, whereas TEM can detect the presence of minute or widely-scattered particles. Thus the x-rays failed to detect the micro-precipitates at the cell boundaries of as-spun ribbons, or the early stages of precipitation within the cells. However, the x-ray diffraction revealed a large difference between the thin and thick 5 wt.% Mn ribbons with respect to the relative abundance of the precipitate phases after long anneals, whereas TEM included a much smaller difference. This may be a result of selective observations by TEM, in that the thick 5 wt.% Mn

ribbon was quite irregular in thickness and the TEM observations were necessarily confined to the thinnest parts of the ribbon.

At compositions up to 5 wt.% Mn, the as-spun ribbons showed no microsegregation and the lattice parameter indicated that all of the manganese was incorporated into the solid solution. At compositions greater than 5 wt.% Mn, or in thicker 5 wt.% Mn ribbons, a cellular or subgrain structure was present in the as-spun ribbons. Very small (~10nm diameter) precipitates were present along the cell or subgrain boundaries, and the concentration of Mn in solid solution within the cells was slightly less than the nominal composition of the sample. At 12 wt.% Mn the samples contained localized regions near the cell walls with dissolved manganese concentration less than that within the cell interiors. At 15 wt.% Mn, the ribbons contained both a solid solution containing close to the nominal concentration of Mn and other Al phase material with a much lower concentration of Mn, plus a significant volume fraction of precipitates.

Upon annealing at 450°C, precipitates grow rapidly at the cell boundaries. It is not clear if the very small precipitates present in the as-spun ribbons are the direct precursors of the rapidly growing precipitates. When more than about 4 wt.% Mn is in solid solution, precipitates also form within the cells but a denuded zone occurs adjacent to the cell boundaries.

We conclude that the cell boundaries, when present, acted as a high diffusivity network by means of which manganese

moved to produce a rapid coarsening of precipitate particles lying along these boundaries. That this process has already started during the cooling of the ribbons after melt spinning is shown by the presence in the as-spun ribbons of the fine precipitates along the cell boundaries, the lattice parameter evidence in the Aℓ-12 wt.% Mn as-spun ribbon of localized regions with lower manganese composition, and the presence of a zone denuded of precipitates adjacent to the boundaries after short anneals.

Hood and Schultz [18] measured a diffusion coefficient of about 10^{13} cm^2/s for Mn in Aℓ at 450°C and saw no difference in the rates for single crystal and polycrystal samples. They, therefore, concluded that diffusion along grain boundaries was not playing an important role. Buckle [19] earlier reported that the diffusion coefficient of Mn in Aℓ decreases rapidly with increasing Mn content. Hood and Shultz found no such effect when they compared the diffusion rate in a sample doped with 0.25% Mn to the rates in very dilute samples. However, as the manganese-doped sample was a single crystal, its composition was much less than those of our samples, and the diffusion rate measurements on it were carried out at temperatures of 579°C or higher, the possibility of concentration-dependent or grain-boundary enhanced diffusion in our samples is not ruled out by the measurements of Hood and Schultz.

The G phase, if it ever nucleates on grain or cell boundaries in the less concentrated alloys, either does not grow sufficiently rapidly to attain detectable size before the supersaturation in these regions becomes depleted, or it dissolves in favor of Al_6Mn. Because the G phase is less stable than Al_6Mn at high temperatures, G precipitates are less likely to have formed on the cell boundaries during the cooling after melt spinning. At higher concentrations, however, the locations of the Al_6Mn and G precipitates are interchanged.

In alloys which have neither a cellular structure nor a Mn concentration high enough to cause precipitation within the cells, the supersaturation can persist for many hours. For alloys containing 5 wt.% Mn or more, the supersaturation disappears much more rapidly under the separate effects of rapid diffusion to precipitates along grain or cell boundaries and copious nucleation of one or more phases within the cells. The Al_6Mn, because of its more rapid growth, shows first in the x-ray diffraction, but the G phase becomes evident only after several hours of coarsening.

The G phase is generally regarded as being metastable with respect to Al_6Mn, but for our samples annealed at 450°C the G phase appeared in the x-ray diffraction patterns to be gaining in intensity while Al_6Mn decreased in intensity even at the longest times studied (up to 92 hours in the 3

wt.% Mn sample). Part of this intensity gain may be attributable to the coarsening of the G precipitates, which only after many hours become large enough to produce a strong diffracted intensity. However, our measurements as well as those of other investigators [2, 20] indicate that if the G phase is not stable at 450°C it is very close to being so. Bulk samples containing 3 to 9 wt.% Mn, which had been hot rolled at 600°C and subsequently annealed for 50-100 hours at 450°C, never showed any G phase. This can be attributed to the lack of sufficient supersaturation in these samples to ever nucleate the G phase. The G" and T phases were observed only in the 3 wt.% Mn and 5 wt.% Mn alloys, respectively. They never occurred in large volume fractions and at least the latter was metastable.

V. CONCLUSION

Several precipitate phases form in supersaturated Aℓ-Mn solid solutions prepared by rapid solidification. At 450°C the G phase appears to be slightly more stable at long times than the $Aℓ_6Mn$ and the G" phase. Another phase, designated T was detected in the Aℓ-5 wt.% Mn ribbon, but it was found to be unstable and disappears following short annealing periods. Cellular substructures, if present, play an important role in the precipitation process, and slight variations in the rapid solidification conditions, as in the 5 wt.% Mn ribbons, can determine which phase predominates after long anneals.

ACKNOWLEDGEMENTS

The authors thank Dr. Robert Mehrabian, Director, Center for Materials Sciences, National Bureau of Standards, for useful discussions.

REFERENCES

1. G. Falkenhagen and W. Hofmann, Z. Metal. 43, 69 (1952).
2. K. Little, G. V. Raynor, and W. Hume-Rothery, J. Inst. Met. 73, 83 (1946).
3. E. Nes, S. E. Naess, and R. Hoier, Z. Metal. 63, 248 (1972).
4. W. W. Mullins and R. F. Sekerka, J. Appl. Phys. 35, 444 (1964).
5. P. Furrer and H. Warlimont, Z. Metall. 62, 100 (1971).
6. T. R. Anantharaman, P. Ramachandrarao, C. Suryanarayana, S. Lele and L. Chattopadhyay, Trans. Ind. Inst. of Metals 30, 423 and 434 (1977).
7. H. Jones, Aluminum 54, 274 (1978).
8. R. J. Schaefer, S. R. Coriell, R. Mehrabian, C. Fenimore and F. S. Biancaniello, in Rapidly Solidified Amorphous and Crystalline Alloys, B. H. Kear, B. C. Giessen, and M. Cohen, eds., North Holland, New York, p. 79, 1982.
9. J. Narayan, J. Appl. Phys. 52, 1289 (1981).
10. A. D. I. Nicol, Acta Cryst. 6, 285 (1953).
11. K. Little and W. Hume-Rothery, J. Inst. Met.. 74, 521 (1948).
12. G. Marchand, J. Inst. Met. 73, 747 (1947).
13. O. Izumi, D. Oelschlagel, and A. Nagata, Trans. Japan Inst. Met. 9, 227 (1968).
14. J. Adam and J. B. Rich, Acta Cryst. 7, 813 (1954).
15. I. N. Fridlyander, V. A. Konstantinov, and N. I. Zhurnal, Fizicheskoi Khimii, 30 (7), 1623 (1956).
16. A. A. Yakunin, I. I. Osipov, V. I. Tkach, and A. B. Lysenko, Fiz. Metal. Metalloved 43, 140 (1977).
17. S. P. Bhat, T. R. Ramachandran, and A. K. Jena, J. Mat. Sci. 9, 1759 (1974).
18. G. M. Hood and R. J. Schultz, Phil. Mag. 23, 1479 (1971).
19. H. Buckle, Z. Electrochem. 49, 238 (1943).
20. K. Kusumoto and M. Ohta, Journ. Inst. Poltechn. Osaka Univ. 5 (6), 57 (1954); Nippon Kinzoku Gakki-Si, 18 (8), 466 (1954).